BABAR NOTE 436 PHYSYCS
July 2, 1998

Lifetimes with full B reconstruction

Ch. de la Vaissière, H. Briand, Nicolas Regnault [1]

Abstract

A method to evaluate separately the lifetimes of $B^{\pm}$ and $B^0/\overline{B}^0$ mesons is described. It requires the full reconstruction of one B meson in the Υ_{4S} decay. The decay vertices of the reconstructed B, of the other B and the Υ_{4S} production point (assumed to belong to a beam-spot ellipse) are connected assuming the direction of their lines of flight from kinematics. A combined fit provides two observables per event connected to lifetimes. The method has been tested on two samples of 4000 $B^{\pm} \to \psi K^{\pm}$ and $B^0 \to \psi K^{\pm}\pi^{\mp}$ decays generated by ASLUND and on a small subsample of 2000 BBSIM events processed through BETA .

An appendix gives details about the fitting procedures.

[1]LPNHE, Laboratoire de Physique Nucleaire des Hautes Energies, Universités Paris VI et VII, Paris.

1 Introduction

The $\Upsilon(4S)$ decays exclusively to pairs of charged or neutral B mesons. For lifetimes measurements, this simple configuration has the complication that no particles comes out of the $\Upsilon(4S)$ decay point which is not measurable in principle. To measure lifetimes without knowing where the B mesons are produced one can use ΔZ , the difference of decay paths between the two mesons projected on the beam axis. The difficulty at this stage is to identify the trajectories attached to these decay points. The particles produced in the subsequent decays of charm mesons have to be recognized. In the most common case, trajectories are to be sorted out between four vertices grouped in two decay chains. Finally, a distinct measurement of the lifetime of charged and neutral B requires a clear identification of $B^{\pm}$s and $B^0/\overline{B}^0$s.

Some of these problems can be reduced when one of the two B mesons is fully reconstructed. The full reconstruction insures a perfect separation between $B^{\pm}$ and $B^0/\overline{B}^0$ pairs by their electric charge and a partition of particles between the two decay chains. Also, the kinematics of the Υ_{4S} desintegration is determined. The direction of the lines of flight of the B mesons are known which allows in principle a determination of their production point.

The critical point is the efficiency of such a reconstruction. It shoud not be too small in order to achieve a significant statistical accuracy. Aslund simulation suggests that one can detect 0.288 D mesons per $B^0\overline{B}^0$ event (153 $D^{\pm}$ and 423 D^0 for 2000 events), and 0.092 B^0 meson per D meson. Therefore, according to that evalulation, one can expect a full B reconstruction efficiency of $\simeq 2.8\%$. By fully detected, it is meant that all the decay products of a D or B meson have been measured in the detectors (this includes at this moment $\pi^{\pm}$, $K^{\pm}$, π^0 but not K^0_s). The upper limit above does not account for the particle identification problems and the efficiencies of the cuts required to select D and B signals above a combinatorial background. The rate of *reconstructible* B mesons is likely to be of the order of 1% or a few per mil.

We have tested the method described below on two particular decay modes $B^{\pm} \to \psi K^{\pm}$ and $B^0 \to \psi K^{\pm}\pi^{\mp}$. They should be considered as example of reconstructed channels. In this preliminary work, the correction due to mixing in the time dependance of the B_d^O decay has not been considered.

2 Principle of the method

The Fig.1 summarizes the peculiar features of the Υ_{4S} decay, after the Lorentz boost along the Z axis due to the machine asymmetry. This boost is characterized by $\beta_{\Upsilon} = 0.4887$ and $\Gamma_{\Upsilon} = 1.1462$. The production point ($x^{\Upsilon}$,$y^{\Upsilon}$,$z^{\Upsilon}$) of the Υ_{4S} belongs to the beam spot ellipse, so that the x^{Υ} and y^{Υ} coordinates are known with an accuracy of $\simeq 140\mu m$ and $\simeq 6\mu m$ respectively, while the z coordinate is affected of a much larger uncertainty of $\simeq 1\ cm$. The pair of B mesons quasi at rest in the Υ_{4S} frame generates a very pinched geometry. The maximal transverse momentum $\overline{P_B} \simeq 0.3247$ GeV is small compared to the B mass $M_B = 5.279 GeV$ The maximal variation of the longitudinal component P_z around its average value $< P_z >$ of 2.962 GeV/c is $\Delta P_z^{max} = 0.3716\ GeV/c$. The maximum angle between the two lines of flight is 0.214 rad (12.3^0).

Each of the two mesons lives with a proper time $c\tau$ and decays. It is convenient to

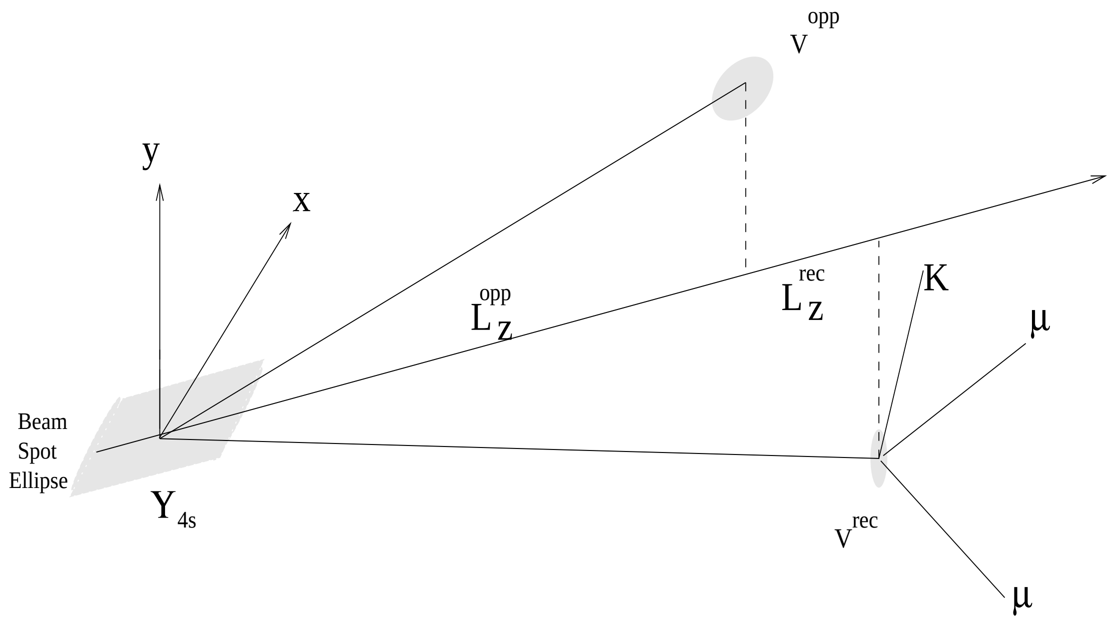

Figure 1: Geometry of the Υ_{4S} decay into a pair of B mesons, one being fully reconstructed. V^{rec} and V^{opp} are the positions of the decays of the reconstructed and opposite Bs. The shaded area around represents the errors on these positions. The Υ_{4S} point belongs to the beam spot ellipse and the directions of the lines connecting Υ_{4S} to V^{rec} and V^{opp} are known from kinematics.

relate $c\tau$ to the z component of the decay path $L_z = z^{decay} - z^{\Upsilon}$,

$$c\tau = L_z \frac{M_B}{P_z} \tag{1}$$

Let us assume that one of the two mesons is fully reconstructed. The recoiling B meson, will be called opposite and labelled "opp", the other being labelled "rec". With these notations the positions of the two B decays are $(\mathrm{x}^{\mathrm{rec}}, \mathrm{y}^{\mathrm{rec}}, \mathrm{z}^{\mathrm{rec}})$ and $(\mathrm{x}^{\mathrm{opp}}, \mathrm{y}^{\mathrm{opp}}, \mathrm{z}^{\mathrm{opp}})$.

Fully reconstructing one B meson means that all particles associated to its decay chain are detected and properly assigned to a vertex of the chain. The quadrimomentum of the reconstructed B, its boost and the direction of its line of flight, are obtained by summing the quadrimomenta of its decay products. The accuracy on these quantities is improved by adding kinematical constraints to the standard geometrical fit of the decay vertex.

In the case of the channels $B^0_d/\overline{B^0_d} \to \psi(\mu^+\mu^-)K^{\mp}\pi^{\pm}$ and $B^{\pm} \to \psi(\mu^+\mu^-)K^{\pm}$ the situation is simple : there is no neutral, nor subsequent charm decays ; all tracks belong to one single vertex. Three kinematical constraints - M_B,M_{ψ}, E_{beam} (beam energy constraint evaluated in the centre of mass) - can be applied. These constraints, added to a strong signature of a muon pair, should insure a clean sample.

2.1 Beam spot fit

The position V^{rec} of the decay of the reconstructed B and its quadrimomentum are estimated by a vertex fit whith three kinematical constraints (See Appendix). This fit is highly constrained : 6 constraints in the $\mathrm{B}^{\pm}$ case, 8 in B^0 or $\overline{\mathrm{B}^0}$ case. It provides accuracy on the $\mathrm{x}^{\mathrm{rec}}, \mathrm{y}^{\mathrm{rec}}, \mathrm{z}^{\mathrm{rec}}$ coordinates and the $\mathrm{P}^{\mathrm{rec}}_{\mathrm{x}}$, $\mathrm{P}^{\mathrm{rec}}_{\mathrm{y}}$,$\mathrm{P}^{\mathrm{rec}}_{\mathrm{z}}$ momentum components. The

Υ_{4S} production point belongs to a very flat beam spot ribbon. Therefore, the decay path L_z^{opp} can be extracted from a second fit insuring that the direction of the line connecting the Υ_{4S} and V^{rec} points is given by the fitted momentum of the reconstructed B. In the approximation where $\sigma(y^{\Upsilon}) \simeq 0$

$$L_z^{rec} \simeq \frac{(y^{rec} - y^{\Upsilon})}{P_y^{rec}/P_z^{rec}} \quad \text{and} \quad c\tau^{rec} = \frac{M_B\ (y^{rec} - y^{\Upsilon})}{P_y^{rec}} \tag{2}$$

As given on tab.1-b, the angle $tg\ \epsilon_y = (P_y/P_z)^{rec}$, whose maximum value is 0.108 rad, is known with an average precision of 1.8 $mrad$. The dominant factor is the accuracy $\sigma(y^{rec})$ on y^{rec}. The pole at $tg\epsilon_y = 0$ in the denominator is avoided by an upper bound on $\sigma(L_z^{rec}) \simeq \sigma(y^{rec})/\text{tg}\ \epsilon_y$. The error $\sigma(L_z)$ after this cut is around 10 times the error on y^{rec}. Despite its low accuracy, the "beam-spot" fit offer the advantage of simplicity and do not require any hypothesis on the *opposite* side.

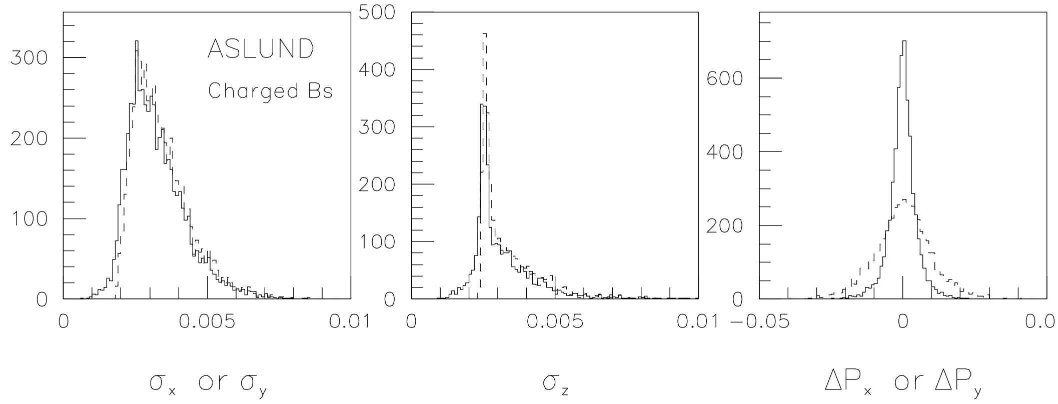

Figure 2: Quality of the vertex and momentum the reconstructed B due to the geometrical and kinematical constraints : a and b) Errors on x_{rec}/y_{rec} and z_{rec} coordinates expressed in cm , the full histograms showing the effect of adding three kinematical constraints to a pure geometrical fit (dashed lines); c) Residue in Gev/c of the P_x^{rec} and P_y^{rec} components.

2.2 Fit connecting the *reconstructed* and *opposite* vertices

One can improve the "mono-side" measurement of $c\tau^{rec}$ by adding further constraints on the *opposite* side. The quadrimomentum, boost and direction of the opposite B are determined from energy and momentum conservation. But there is at this stage the difficulty of distinguishing between "primary" B-tracks belonging to the B decay itself and "secondaries" associated to D mesons. D^0 mesons have a rather short lifetime and travel little. Most of the tracks associated to a D^0 may look attached to the main B vertex. Charged $D^{\pm}$ have longer $c\tau$, but undergo generally 1-prong decays. Therefore, we attempt to fit all the *opposite* tracks to a single vertex. If the probability of this geometrical fit is $> 1\%$, we take the result with its error matrix as a first approximation of $x^{opp}, y^{opp}, z^{opp}$.

Once the first order approximation of V_{opp} has been calculated, a "combined" fit of the 3 points is attempted, assuming from kinematics the direction of the lines of flight and requiring the Υ_{4S} point to belong to the beam spot ribbon. The "combined" fit (detailed in the appendix) provides the measurement of the decay paths L_z^{rec} and L_z^{opp}, compared to L_z^{rec} only with the beam spot fit.

Owing to the pinched geometry, the measured values of L_z^{rec} and L_z^{opp} have a positive correlation close to 1. The angle between the two line of flight being twice that of the simple beam spot case, the error on $c\tau$ are improved. It is convenient to introduce the sum and the difference of the two decay paths. The sum $\Sigma L_z = L_z^{opp} + L_z^{rec}$ is measured with an accuracy practically double that of the individual paths, but the average value of this quantity gives directly the lifetime in the absence of biasses and background. In the difference $\Delta Z = L_z^{opp} - L_z^{rec}$, the effect of the correlation is basically removed. This is the most accurate observable. However the distribution is symmetric with respect to 0 and the lifetime can only be estimated from the shape of the distribution.

Knowing the boost or equivalently the polar angle $\overline{\theta}$ of the opposite B in the center of mass, the L_z^{rec} and L_z^{opp} can be transformed into the difference and sum of the proper times $c\tau^{rec}$ and $c\tau^{opp}$,

$$\Sigma c\tau = \frac{M_B}{P_z^{rec}\ P_z^{opp}}(< P_z > \Sigma L_z - \Delta P_z^{max} cos\overline{\theta}\ \Delta Z) \tag{3}$$

$$\Delta c\tau = \frac{M_B}{P_z^{rec}\ P_z^{opp}}(< P_z > \Delta Z - \Delta P_z^{max} cos\overline{\theta}\ \Sigma L_z) \tag{4}$$

Numerically

$$\Sigma c\tau \simeq 1.782\ (\Sigma L_z - 0.125\ cos\overline{\theta}\ \Delta Z) \tag{5}$$

$$\Delta c\tau \simeq 1.782\ (\Delta Z - 0.125\ cos\overline{\theta}\ \Sigma L_z) \tag{6}$$

3 Results on Lifetimes obtained from the fast ASLUND simulation

The results presented in this section are based on 4000 $B^{\pm} \to \psi(\mu^+\mu^-)K^{\pm}$ and $B_d^0/\overline{B_d^0} \to \psi(\mu^+\mu^-)K^{\mp}\pi^{\pm}$ decays generated by ASLUND. Track reconstruction, acceptance, momentum cuts reduces the number of reconstructed Bs to 2840/2550 respectively.

In the case of the simple beam spot fit, the pole at $tg\epsilon_y = 0$ is avoided by the condition $\sigma(L_z^{rec}) < 800\mu$m. This reduces the number of useful decays to 1422(1266) respectively. In the case of the combined fit, we require $|cos\overline{\theta}| < 0.80$, at least three charged detected tracks for the opposite B, probability of the geometrical (on the opposite side) and combined fits above 1%. The probability distributions of the two vertex fits are shown on Fig.3. Around 30% of *opposite* vertices are eliminated by the 1% probability cut (Fig.3-b). The spike at low probability is due to the difficulty to fit a single vertex contaminated by tracks coming from charm and eventually from K_s^0. Some of these vertices can be recovered by eliminating tracks with the higher contribuition to the χ^2. After this recovery, the total numbers of events with measurements reduces to 1749($B^{\pm}$) and (1384 ($B^0/\overline{B^0}$).

The upper part of the table 1 summarises the accuracy achieved on the *reconstructed* side by the geometrical fit with kinematical constraints, and on the *opposite* side by the

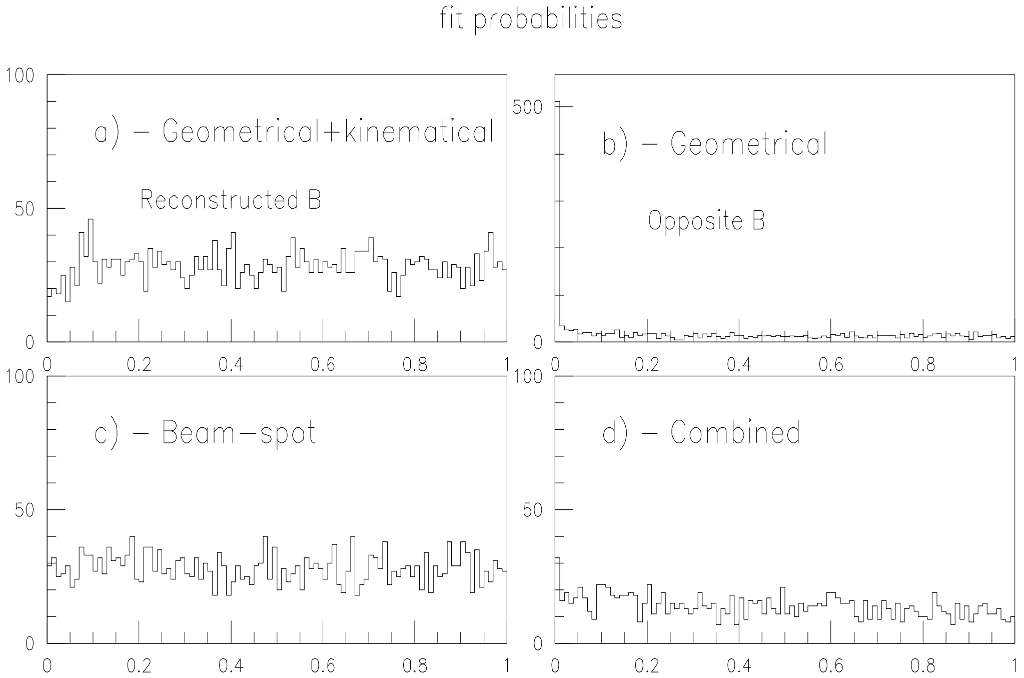

Figure 3: Fit probabilities: a) ;b) vertex fit on opposite side; c) lifetime beam-spot fit ;b) lifetime combined fit.

geometrical fit which neglects subsequent charm decays. The outputs of the separate vertexing of the two Bs are the input of the lifetimes fits whose principles have been given in the previous section. The table 1-b shows the accuracies achieved on the momentum components $\mathrm{P_x^{rec}}$, $\mathrm{P_y^{rec}}$, $\mathrm{P_z^{rec}}$. The direction of the lines of flight is reproduced with an average 1.8 mrad precision. The determination of the position of the vertex on the *reconstructed* side is accurate, because the multiplicity is low in the $B^{\pm} \rightarrow \psi K^{\pm}$ and $B^0 \rightarrow \psi K^{\pm}\pi^{\mp}$ modes. The decay products have momenta higher than average which reduces the degradation of the multiple scattering. The fig.2-b shows that an average resolution of about 33 μm, can be achieved in the z_{rec} coordinate with a rather long tail. The introduction of the kinematical constraints improve mainly the resolution of the B^{rec} quadrimomentum (rms of 4 MeV/c in P_x, P_y), but has less impact on geometrical errors. The accuracy on the coordinates of the opposite vertex by a mere geometrical fit are are poorer, $\simeq 100\mu m$ in average. Furthermore, the coordinate $\mathrm{z^{opp}}$ is affected by a $\simeq 20(25)\mu m$ positive bias due to the inclusion of charm tracks in the fit. This bias has to be taken into account in the determination of lifetimes.

The table 1-c shows the accuracies obtained after the combined fit of the two vertices position and the beam spot. Connecting the two points increases dramatically the accuracies in the x,y coordinates, but have little effect on $\mathrm{z^{rec}}$ and $\mathrm{z^{opp}}$. The table 1-d compares the accuracies obtained on the lifetime observables by the "beam spot" and the "combined" fit.

In the case of the beam-spot algorithm, the Fig.4.a shows the distribution of $\sigma(c\tau^{rec})$

$\mathrm{x}^{\mathrm{rec}}$	$\mathrm{y}^{\mathrm{rec}}$	$\mathrm{z}^{\mathrm{rec}}$	$\mathrm{x}^{\mathrm{opp}}$	$\mathrm{y}^{\mathrm{opp}}$	$\mathrm{z}^{\mathrm{opp}}$	a)Separate vertexing
32 μm	32 μm	31μm	98 μm	96 μm	98μm	$B^{\pm}$
34 μm	34 μm	33μm	102 μm	98 μm	107μm	B^0
P_x or P_y	P_z			ϵ_{xy}	$cos\overline{\theta}$	b)Kinematics
4.9 MeV/c	5.1 MeV/c			1.8 mrad	0.015	$B^{\pm}$
4.9 MeV/c	5.0 MeV/c			1.8 mrad	0.015	B^0
x_{rec}	$\mathrm{y}^{\mathrm{rec}}$	$\mathrm{z}^{\mathrm{rec}}$	$\mathrm{x}^{\mathrm{opp}}$	$\mathrm{y}^{\mathrm{opp}}$	$\mathrm{z}^{\mathrm{opp}}$	c) Connected vertexing
29 μm	21 μm	33 μm	54 μm	25 μm	89 μm	$B^{\pm}$
31 μm	25 μm	35 μm	57 μm	27 μm	96 μm	B^0
$c\tau^{rec}_{b.spot}$			$c\tau^{rec}_{comb.}$	$\Delta c\tau$	$\Sigma c\tau$	d) lifetimes observables
755 μm			583 μm	158 μm	1170 μm	$B^{\pm}$
780 μm			611 μm	162 μm	1213 μm	B^0

Table 1: Errors summary: a) rms on vertex residuals obtained from a separated vertexing of the *reconstructed* and *opposite* B mesons ; b) rms of the residuals on the B_{rec} momentum components and of the line of flight direction due to the kinematical constraints. c) rms on vertex residuals after connecting the B_{rec}, the Υ_{4S} and the B_{opp} vertices by "combined" fit ; d) Average error on the two estimations of $c\tau^{rec}$, $\Delta c\tau$ and $\Sigma c\tau$.

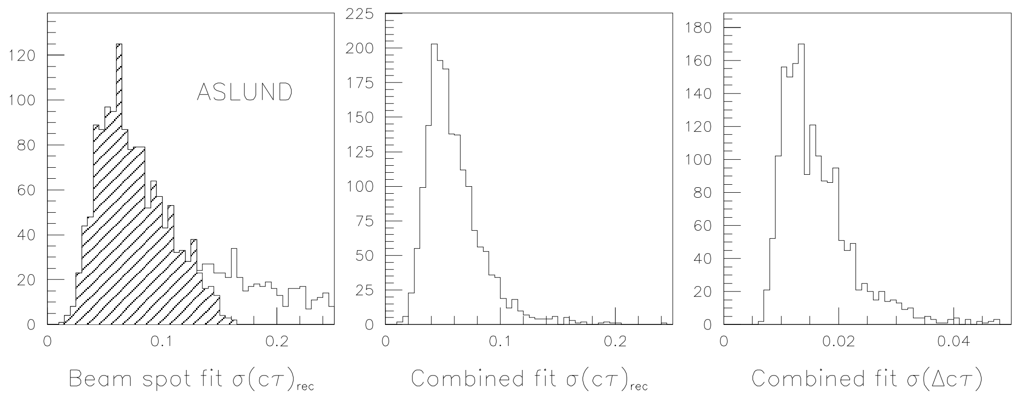

Figure 4: Distribution for $B^{\pm}$ lifetimes of the errors on : (a) $c\tau_{rec}$ in the case of the beam-spot fit (the shaded area shows the effect of the cut $\sigma(L_z) < 800\mu m$): b) $c\tau_{rec}$ and $\Delta c\tau$ in the case of the "combined fit"

and the Figs.5-a and 6-a that of $c\tau^{rec}$. The average value of the observable $c\tau^{rec}$ is an unbiassed estimator of the lifetime. It is found to be $465 \pm 25\mu m$ for $B^{\pm}$ and $471 \pm 27\mu m$ for B^0 to be compared with the expectation of $450\mu m$. A maximum likelihood fit of the $c\tau$ distribution by an exponential convoluted by a gaussian whose width $\sigma(c\tau)$ calculated event by event gives consistent values. The beam spot technique can be used whenever a B is reconstructed. The dominant factor is the accuracy on $\mathrm{y}^{\mathrm{rec}}$, which depends on the decay mode. Assuming that this error is $50\mu m$ for standard reconstructed decay modes, one may expect an accuracy of $8\mu m$ per 100K reconstructed decays.

	Method	Stat	M.L. $c\tau$ fit	average $c\tau$
$B^{\pm}$	Beam spot	1422	455 ± 27	465 ± 25
	$c\tau^{rec}$ side	1731	461 ± 21	452 ± 20
	$c\tau^{opp}$ side	—	—	486 ± 20
	$\Delta c\tau$	1660	421 ± 19	
	$\Sigma c\tau$	—	—	457 ± 22 verifier
B^0	Beam spot	1266	462 ± 29	471 ± 27
	$c\tau^{rec}$ side	1367.	446 ± 26	433 ± 23
	$c\tau^{opp}$ side	1147.		491 ± 24
	$\Delta c\tau$	1660	441 ± 19	
	$\Sigma c\tau$	—		472 ± 22

Table 2: Comparison of the evaluations of $c\tau$ extracted from a maximum likelihood fit or given by the average of observables.The expected value is $450\mu m$

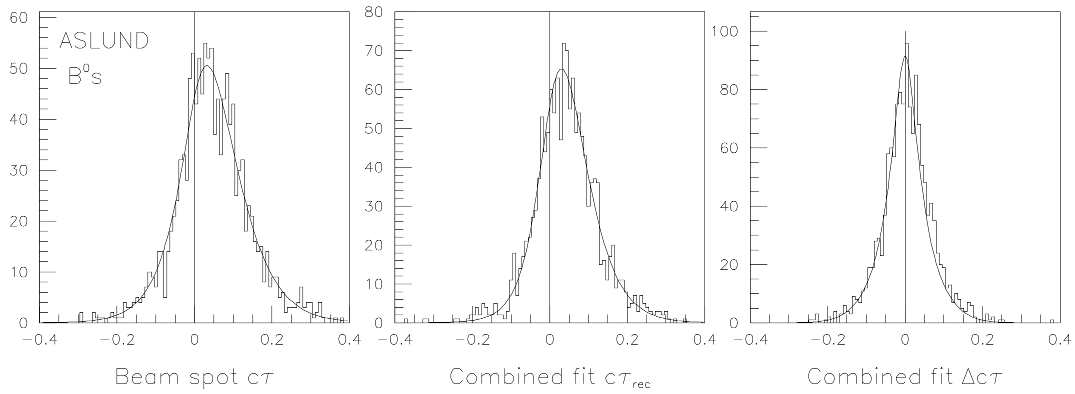

Figure 5: Distribution of lifetimes observables $c\tau^{rec}$ and $\Delta C\tau$ for neutral Bs.

The "combined" fit improves the "beam spot" measurement. It provides two data per useful event. It is interesting to observe on tab.2 that the positive bias of z_{opp} (due to D tracks pollution) which affects $c\tau^{opp}$ has practically no effect on the *reconstructed* side. $c\tau^{rec}$ is a useful observable. Its average value appears a good estimator of the lifetime. A maximum likelihood fit gives consistent results: 461 ± 21 and 446 ± 26 for charged and neutral Bs.

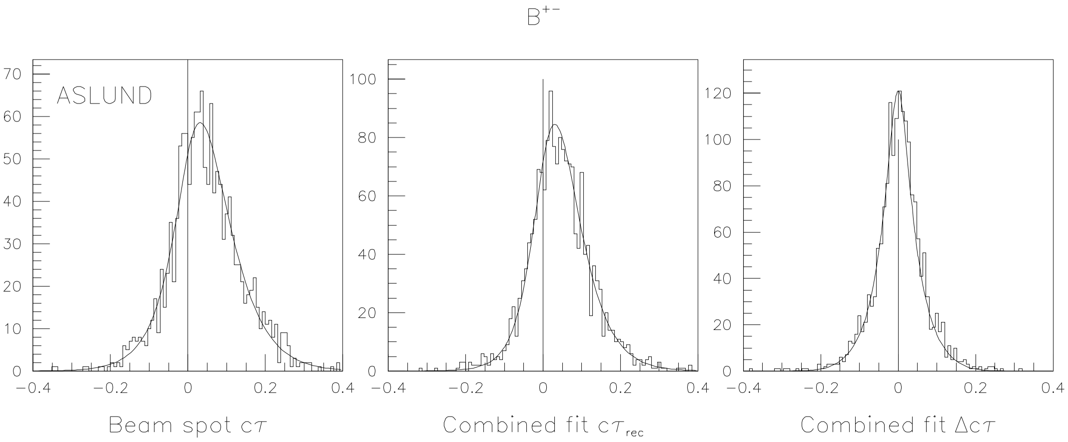

Figure 6: Distribution of lifetimes observables $c\tau^{rec}$ and $\Delta C\tau$ for charged Bs.

One can use also the accurate observable $\Delta c\tau$. According to the tab.1-d the error on $\Delta c\tau$ is three to four times smaller than the error on $c\tau_{rec}$. Being a difference of lifetime, the average $< \Delta c\tau >$ is expected to be 0 and can not be used to estimate the average $< c\tau >$, which has then to be extracted by an unbinned maximun likelihood fit. This fit assumes a negative and positive exponentials, convoluted by the "event by event" error. The observed averages of $< \Delta c\tau >$ are 25 ± 17 μm for $\mathrm{B}^{\pm}$ and 50 ± 20 μm for B^0. These positive values are related to the bias on $c\tau^{opp}$ mentionned above. This bias can be introduced as a parameter in the maximum likelihood fit. It can be also evaluated or corrected using simulation. Within the limited statistics of the studied sample, it seems to have marginal effects.

To improve accuracy, one can finally combines two measurements. The best combination is probably the accurate but biassed $\Delta c\tau$ observable with the bias free $c\tau_{rec}$ observable. The first quantity is a difference of decay paths, while the other is a decay path. The correlations are null in average. They remains moderate at the event level. It is therefore legitimate to combine the two corresponding measurements. By doing so, we obtain $< \tau >= 1.463 \pm 0.047$ ps for $\mathrm{B}^{\pm}$ and $< \tau >= 1.476 \pm 0.051$ ps for $\mathrm{B}^0/\overline{\mathrm{B}^0}$ with these dedicated samples of 4000 decays.

4 Preliminary results with full reconstruction

A preliminary sample of 2000 $\mathrm{B}^0/\overline{\mathrm{B}^0}$ dedicated events was generated by BBSIM and stored on a BEAST tape [2] Among them 460, were succesfully reconstructed by BETA and have been processed to the same analysis than the event generated by Aslund.

The Fig. 7 compares between ASLUND and BBSIM the errors on vertexing and the Fig.8 the errors on the main lifetimes observables. The main difference with ASLUND appears to be a stronger loss of events: a factor 6 in statistics. The BBSIM events, being more realistic, have more difficulties to pass the reconstruction phase in BETA and

[2] In BBSIM data, the essential of the losses seems to come from tracks not found in the reconstruction

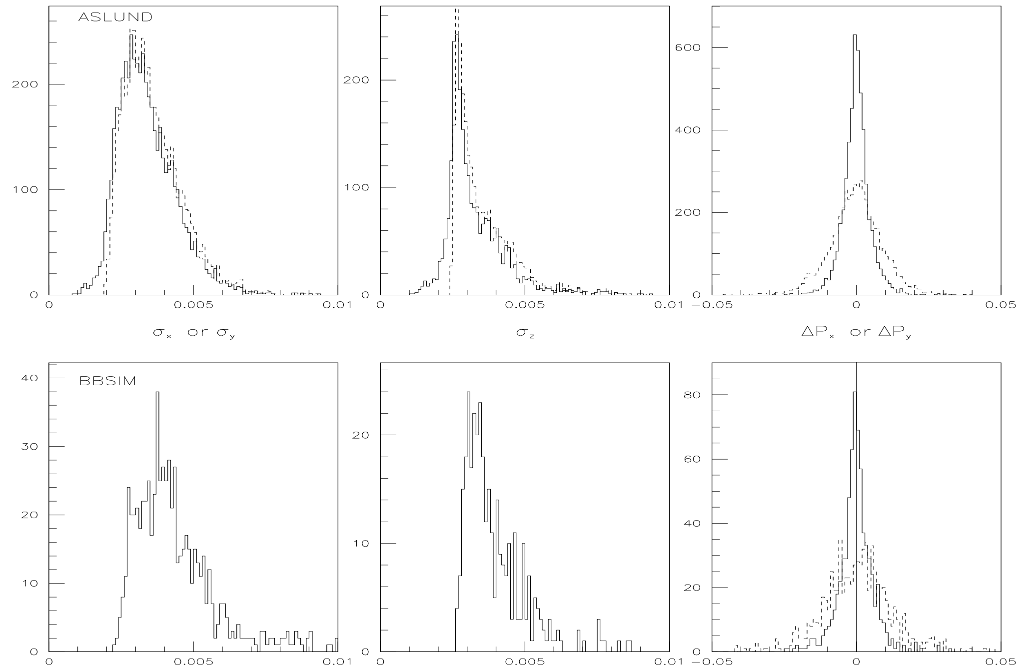

Figure 7: Same as Fig.2. Comparison between ASLUND and BBSIM of the quality of the vertex and momentum of the reconstructed B due to the geometrical and kinematical constraints : a and b) Errors on x_{rec}/y_{rec} and z_{rec} coordinates expressed in cm; c) Residue in Gev/c of the $\mathrm{P_x^{rec}}$ and $\mathrm{P_y^{rec}}$ components.

the selection cuts. While around 50% of events are found useful for the analysis with ASLUND, this proportion is less than 20% with BBSIM.

The low statistics available with the actual BBSIM sample makes detailed comparison difficult. However, it can be seen, once events are selected, they are comparable in quality with those of ASLUND. The distributions of errors shows only a limited degradation of accuracy.

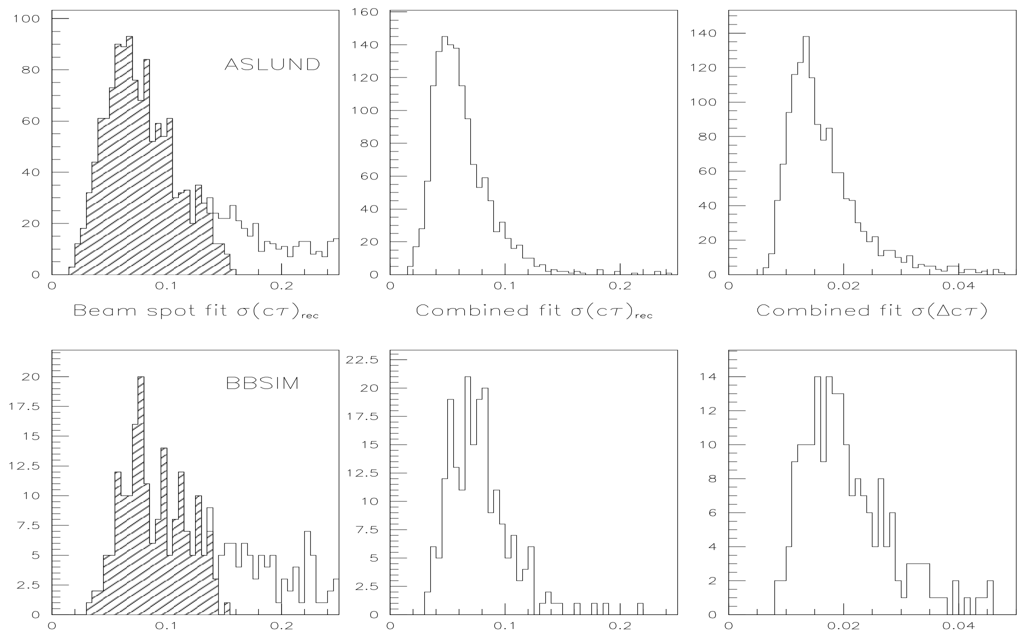

Figure 8: Comparison of errors on the 3 main of lifetimes observables between ASLUND and BBSIM

The Fig. 9 compares the lifetime observables themselves and the tab.3 summarizes the results obtained on average lifetime for this reduced sample.

	Method	Stat	M.L. $c\tau$ fit	average $c\tau$
B^0	Beam spot	185	479 -93 + 77	463 $\pm$ 83
	$c\tau^{rec}$ side	201	517 $\pm$ 62	537 $\pm$ 71
	$c\tau^{opp}$ side	—		521 $\pm$ 76
	$\Delta c\tau$	172	449 $\pm$ 53	
	$\Sigma c\tau$	—		555 $\pm$ 72

Table 3: Measurements of $c\tau$ for the lifetimes observables , obtained with the 205 useful BBSIM events

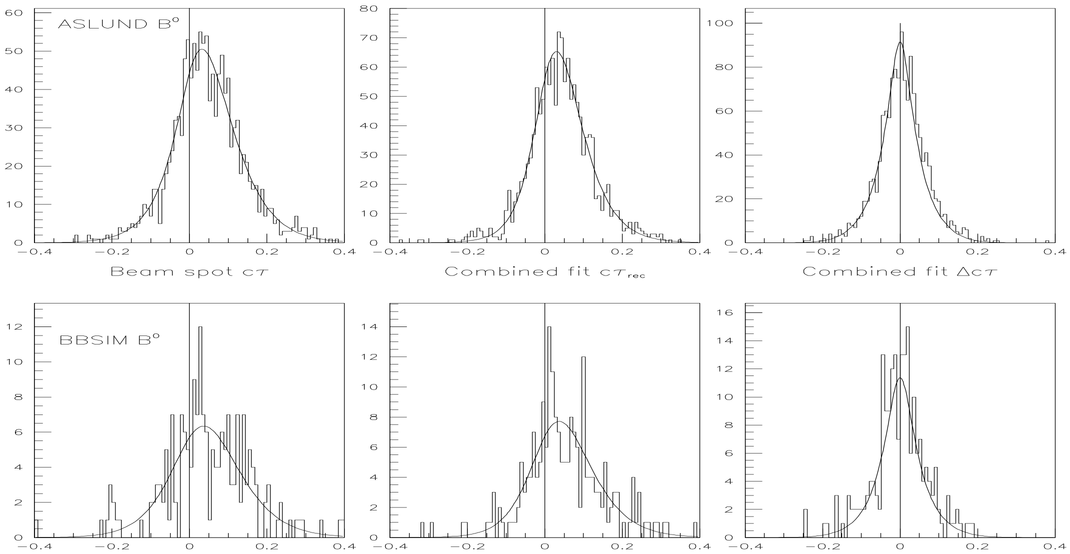

Figure 9: Comparison between ASLUND and BBSIM of the lifetimes observables $c\tau^{rec}$ and $\Delta C\tau$ in the case $\mathrm{B}^0/\overline{\mathrm{B}^0}$.

Combining the $c\tau_{rec}$ and $\Delta c\tau$ Measurements as before gives $< c\tau >= 477 \pm 40\ \mu m$. With a low statistics of around 200 evts one is able to measure the lifetime wit a 8% statistical error.

5 Conclusions

The advantage of the $\Psi \rightarrow \mu\mu$ events is to use a clean signature in addition of the selectivity proper to the 3 kinematical constraints. It is likely that for such channels the level of background will be low. A study of background effects, which are the main likely source of systematics, remains however to be done. An other advantage proper to the *reconstructed* channels, is to be sure to measure either the $\mathrm{B}^0/\overline{\mathrm{B}^0}$ or $\mathrm{B}^{\pm}$ lifetime, and to sort out tracks coming from this B and its *opposite* partner. The disadvantage of the two "golden" channels considered is their low branching ratio. If one is able to reconstruct π^0s, one may expect to extend somewhat the size of the sample. A natural extension would be to use standard decays involving identified D and D^* mesons. They offer good signature, but owing to a decay chain, the determination of the B decay vertex is more complex. We intend to investigate them in the next step. This requires an extension of the present geometrical+kinematical fit allowing for subsequent charm decays and D^*s.

The evaluation of lifetimes requires a good alignement and a good understanding of tracking. This more important in the case of the $\Delta c\tau$ than for $c\tau_{rec}$, since for this observable one can use the average of this quantity to evaluate the lifetime, estimator in principle not affected, in the absence of background, by a poor estimation of errors.

An eventual bias on the y position of the beam-spot, can be controlled on data itself, by comparing the topologies when $\mathrm{P}_{\mathrm{y}}^{\mathrm{rec}} > 0$ and $\mathrm{P}_{\mathrm{y}}^{\mathrm{rec}} < 0$.

One can finally use partially reconstructed Bs to increase the statistics. Semi-leptonic decays offer the best opportunities, since leptons associated to a D or D^* gives clean and relatively abundant signatures. The problem is to be sure of the charge of the B and of the separation of the tracks between the $semi-reconstructed$ B and its partner. Simulation shows that the $D^{*\pm}$ are much more connected to $B^0/\overline{B^0}$ than $B^{\pm}$. This should allows some separation of the lifetimes. A study is under developpement.

References

[1] Statistical and Computational Methods in Data Analysis, Siegmund Brandt, North Holland Publishing company, Second edition, 1976, page 221-223.

Appendix A: Fit description

The geometrical+kinematical fit of the reconstructed B, the beam spot and combined fits for the lifetimes were performed by a unique and fast fitting FORTRAN package called FITGEOKIN. It is essentially a one step least squares minimisation of parameters q, with unknowns η and constraints $F(q,\eta)_r = 0$. The minimization is performed, using the formalism of Lagrange multipliers, of

$$\sum_{i,j} W_{i,j} dq_i dq_j + \sum_r \mu_r F(q,\eta)_r \tag{7}$$

where $\tilde{W}$ is the parameters weight matrix inverse of the error matrix $\tilde{\Sigma}$ and μ_r are Lagrange multipliers. The mathematics can be found in the reference [1].

The parameters entering in the fit are grouped into independant subsets : tracks, beam-spot coordinates, vertex coordinates, π^0s, etc... The total error matrix has a bloc diagonal structure which accelerates inversion and matrix multiplication

The constraints are assumed quasi-linear. They are evaluated for the unfitted values of the parameters $\hat{q}$ and starting values $\hat{\eta}$ of the unknowns. To first order constraint r is :

$$F(q,\eta)_r = F(\hat{q},\hat{\eta})_r + \sum_i \frac{\partial F(\hat{q},\hat{\eta})_r}{\partial q_i} dq_i + \sum_u \frac{\partial F(\hat{q},\hat{\eta})_r}{\partial \eta_u} d\eta_u = 0 \tag{8}$$

Besides the set $F(\hat{q},\hat{\eta})_r$, one has to enter two matrices of first order derivatives with respect to the parameters and the unknowns. Generally these matrices contains many zeroes (For example in the case of the two geometrical constraints relative to a given track, all the elements corresponding to the parameters of the other tracks are null).

It is assumed that the initial values of the parameters are close to the truth. For example in the case of a $B^\pm$, one attempts the geometrical+kinematical fit only if a preliminary geometrical vertexing of the μ^+, μ^-, and $K^\pm$ tracks has already been successful, if the masses $M(\mu^+\mu^-)$ and $M(\mu^+\mu^-K^\pm)$ are close to M_ψ and M_B, and if the beam energy constraint is almost verified. With this precaution, the least square minimisation converges in one iteration. To give an idea of its rapidity, in the example of ASLUND, FITGEOKIN is called 7725 times in 4000 $B^\pm$ evts (2840 geometrical+kinematical fit, 2816 beam-spot fit, 2069 combined fits). The execution time on an AIX station, around 1 minutes, is not found sensitive to the amount of fitting.

The vertex+kinematical fit of the reconstructed B and three lifetime fits used in this analysis are detailed below.

.1 Geometrical+kinematical fit of the reconstructed B

The characteristics of this fit are :

- 3 Unknowns : x^{rec}, y^{rec}, z^{rec}
- 15 ($B^\pm$) or 20 ($B^0/\overline{B^0}$) parameters with their errors matrices subdivided in 3 or 4 subsets, each set of 5 parameters representing a charged trajectory i. The choice made is : $(\varphi, 1/\rho, \theta, d^0, Z^0)_i$.
- 6 or 8 geometrical constraints and 3 kinematical constraints detailed below. The geometrical+kinematical fit has 6 (8) degrees of freedom.

There is two geometrical constraints per track, Each track is constrained to pass by the vertex $\mathrm{x^{rec}}$, $\mathrm{y^{rec}}$, $\mathrm{z^{rec}}$. One is dealing with decay paths of a few hundreth of microns. A linear representation of the track helix in the vicinity of the beams crossing point is therefore legitimate. In this linear approximation the curvature parameter $1/\rho_i$ does not enter and only the azimuthal parameter φ_i is common to the two constraints.

$$\mathrm{y^{rec}cos\varphi_i - x^{rec}sin\varphi_i + d_i^0 = 0} \tag{9}$$

$$\mathrm{z^{rec} - Z_i^0 - tg\theta_i(x^{rec}cos\varphi_i + y^{rec}sin\varphi_i) = 0} \tag{10}$$

The constraints values and their derivatives are evaluated for the initial values of the parameters and the unknowns. The two matrices of derivatives are given below for the two geometrical constraints relative to a track i (The derivatives with respect to parameters of other tracks being 0.)

Constraint	$\frac{\partial F}{\partial \varphi_i}$	$\frac{\partial F}{\partial c_i}$	$\frac{\partial F}{\partial \theta_i}$	$\frac{\partial F}{\partial d_i^0}$	$\frac{\partial F}{\partial Z_i^0}$	$\frac{\partial F}{\partial \mathrm{x^{rec}}}$	$\frac{\partial F}{\partial \mathrm{y^{rec}}}$	$\frac{\partial F}{\partial \mathrm{z^{rec}}}$
xy_i	$-s_i$	0	0	1	0	-$sin\varphi_i$	-$cos\varphi_i$	0
z_i	$-h_i tg\theta_i$	0	$-s_i(1+tg\theta_i^2)$	0	-1	-$tg\theta_i cos\varphi_i$	-$tg\theta_i sin\varphi_i$	1

Table 4: Derivatives of the geometricals constraints, with respect to the track i parameters and to the unknown coordinates of the vertex. Some derivatives are expressed in terms of $s_i(\mathrm{x^{rec}}, \mathrm{y^{rec}}, \varphi_\mathrm{i}) = \mathrm{x^{rec}cos\varphi_i + y^{rec}sin\varphi_i}$ and $h_i(\mathrm{x^{rec}}, \mathrm{y^{rec}}, \varphi_\mathrm{i}) = \mathrm{y^{rec}cos\varphi_i - x^{rec}sin\varphi_i}$.

The kinematical constraints do not involve the “closest approach” parameters d^0 and Z^0 and are sensitive to curvatures. They link the $\varphi, 1/\rho, \theta$ parameters of several tracks. These are expressed in terms of the quadrimomenta of the contributing particles, whose non-zero derivatives with respect to $\varphi, 1/\rho, \theta$ are tabulated below

	P_x	P_y	P_z	E
$\partial/\partial\varphi$	-P_y	P_x	0	0
$\partial/\partial 1/\rho$	-$P_x\rho$	-$P_y\rho$	-$P_x\rho$	-$P\rho$ (P/E)
$\partial/\partial\theta$	0	0	-P^2/P_{xy}	-P^2P_z/EP_{xy}

Table 5: Derivatives of track quadrimomentum components with respect to trajectory parameters

The contraints expresses that the mass of the $\mu^+\mu^-$ tracks is equal to M_ψ, the mass of the $\mu^+\mu^-K^\pm(\pi^\mp)$ system is equal to M_b, and that the energy of the $\mu^+\mu^-K^\pm(\pi^\mp)$ tracks, transformed in the centre of mass frame, is equal to $\mathrm{\overline{E_B}}$. [3]

$$\frac{(E_{\mu^+}+E_{\mu^-})^2 - (\vec{P_{\mu^+}}+\vec{P_{\mu^-}})^2}{M_\psi^2} - 1 = 0 \tag{11}$$

$$\frac{(\sum_{all} E_i)^2 - (\sum_{all} \vec{P_i})^2}{M_B^2} - 1 = 0 \tag{12}$$

[3]The value of $\mathrm{\overline{E_B}}$ is just a few MeV above M_B. Owing to small energy released in the Υ_{4S} decay, $\overline{P_B}$, the center of mass momentum of the Bs, is very sensitive to $\mathrm{\overline{E_B}}$. To take into account the spread of the beam energy (6 MeV), on can introduce $\mathrm{\overline{E_B}}$ as a parameter instead of a constant.

$$\Gamma_{\Upsilon}\frac{\sum_{\mathrm{all}}(\mathrm{E_i}-\beta_{\Upsilon}\mathrm{P_{z,i}})}{\overline{\mathrm{E_B}}}-1=0 \tag{13}$$

The table gives the constraint derivatives with respect to the parameters q_i of the contributing tracks.

Constraint	$\frac{\partial F}{\partial q_i}$	Particles involved
M_ψ	$\frac{2}{M_\psi^2}(\frac{\partial E_i}{\partial q_i}(E_{\mu^+}+E_{\mu^-})-\frac{\partial \vec{P_i}}{\partial q_i}.(\vec{P_{\mu^+}}+\vec{P_{\mu^-}}))$	μ^+ and μ^-
M_B	$\frac{2}{M_B^2}(\frac{\partial E_i}{\partial q_i}\sum_{all}E_i)-\frac{\partial \vec{P_i}}{\partial q_i}.\sum_{all}\vec{P_i})$	all
$\overline{\mathrm{E_B}}$	$\frac{\Gamma_\Upsilon}{\overline{\mathrm{E_B}}}(\frac{\partial E_i}{\partial q_i}-\beta_\Upsilon\frac{\partial \mathrm{P_{z,i}}}{\partial \mathrm{q_i}})$	all

Table 6: Derivatives of the kinematical constraints, with respect to the track i parameters.

.2 Beam spot fit of $\mathrm{L_z^{rec}}$

The characteristics of the fit are :

- 1 unknown, the decay path : $\mathrm{L_z^{rec}}$
- 5 parameters with their errors matrices grouped in two sets : $\mathrm{x^{rec}}$,$\mathrm{y^{rec}}$,$\mathrm{z^{rec}}$ for the reconstructed vertex and $\mathrm{x^{\Upsilon}}$,$\mathrm{y^{\Upsilon}}$ for the beam spot.
- 2 constraints which are:

$$\mathrm{x^{rec}}-\mathrm{x^{\Upsilon}}-\frac{\mathrm{P_x^{rec}}}{\mathrm{P_z^{rec}}}\mathrm{L_z^{rec}}=0 \tag{14}$$

$$\mathrm{y^{rec}}-\mathrm{y^{\Upsilon}}-\frac{\mathrm{P_x^{rec}}}{\mathrm{P_z^{rec}}}\mathrm{L_z^{rec}}=0 \tag{15}$$

The beam spot fit is a 1-C fit. The initial coordinates of V^{rec} and errors matrices, are the output of the previous fit. The components $\mathrm{P_x^{rec}}$,$\mathrm{P_y^{rec}}$,$\mathrm{P_z^{rec}}$ also and they are considered constant. They define the direction of the line of flight.

Constraint	$\frac{\partial F}{\partial \mathrm{x^{rec}}}$	$\frac{\partial F}{\partial \mathrm{y^{rec}}}$	$\frac{\partial F}{\partial \mathrm{z^{rec}}}$	$\frac{\partial F}{\partial \mathrm{x^{\Upsilon}}}$	$\frac{\partial F}{\partial \mathrm{y^{\Upsilon}}}$	$\frac{\partial F}{\partial \mathrm{L_z^{rec}}}$
$\mathrm{x^{rec}},\mathrm{x^{\Upsilon}}$	1	0	0	-1	0	- $\mathrm{P_x^{rec}}/\mathrm{P_z^{rec}}$
$\mathrm{y^{rec}},\mathrm{y^{\Upsilon}}$	0	1	0	0	-1	- $\mathrm{P_y^{rec}}/\mathrm{P_z^{rec}}$

Table 7: Derivatives of the beamspot fit constraints with respect to the vertex,beamspot parameters and lifetime unknown $\mathrm{L_z^{rec}}$.

.3 Combined fit

The combined fit is a 3-C fit. Its characteristics are :

- 2 unknowns, the decay paths : $\mathrm{L_z^{rec}}$ and $\mathrm{L_z^{opp}}$

- 8 parameters (with their errors matrices) subdivided in 3 subsets : $\mathrm{x}^{\mathrm{rec}}$,$\mathrm{y}^{\mathrm{rec}}$,$\mathrm{z}^{\mathrm{rec}}$ for the reconstructed vertex; x^{Υ},y^{Υ} for the beam spot; and $\mathrm{x}^{\mathrm{opp}}$,$\mathrm{y}^{\mathrm{opp}}$,$\mathrm{z}^{\mathrm{opp}}$ for the opposite vertex.

- 5 geometrical constraints which are :

$$\mathrm{x}^{\mathrm{rec}} - \mathrm{x}^{\Upsilon} - \frac{\mathrm{P}_{\mathrm{x}}^{\mathrm{rec}}}{\mathrm{P}_{\mathrm{z}}^{\mathrm{rec}}} \mathrm{L}_{\mathrm{z}}^{\mathrm{rec}} = 0 \tag{16}$$

$$\mathrm{y}^{\mathrm{rec}} - \mathrm{y}^{\Upsilon} - \frac{\mathrm{P}_{\mathrm{y}}^{\mathrm{rec}}}{\mathrm{P}_{\mathrm{z}}^{\mathrm{rec}}} \mathrm{L}_{\mathrm{z}}^{\mathrm{rec}} = 0 \tag{17}$$

$$\mathrm{x}^{\mathrm{opp}} - \mathrm{x}^{\Upsilon} - \frac{\mathrm{P}_{\mathrm{y}}^{\mathrm{opp}}}{\mathrm{P}_{\mathrm{z}}^{\mathrm{opp}}} \mathrm{L}_{\mathrm{z}}^{\mathrm{opp}} = 0 \tag{18}$$

$$\mathrm{y}^{\mathrm{opp}} - \mathrm{y}^{\Upsilon} - \frac{\mathrm{P}_{\mathrm{y}}^{\mathrm{opp}}}{\mathrm{P}_{\mathrm{z}}^{\mathrm{opp}}} \mathrm{L}_{\mathrm{z}}^{\mathrm{opp}} = 0 \tag{19}$$

$$\mathrm{z}^{\mathrm{opp}} - \mathrm{z}^{\mathrm{rec}} + \mathrm{L}_{\mathrm{z}}^{\mathrm{rec}} - \mathrm{L}_{\mathrm{z}}^{\mathrm{opp}} = 0 \tag{20}$$

The initial coordinates of V^{rec} and V^{opp} (with their errors matrices) are evaluated before by the geometrical+kinematical fit above (V^{rec}) and a geometrical fit (V^{opp}). The following tables gives the two derivative matrices, which are constants.

Constraint	$\frac{\partial F}{\partial \mathrm{L}_{\mathrm{z}}^{\mathrm{rec}}}$	$\frac{\partial F}{\partial \mathrm{L}_{\mathrm{z}}^{\mathrm{opp}}}$
$\mathrm{x}^{\mathrm{rec}}, \mathrm{x}^{\Upsilon}$	$-\ \mathrm{P}_{\mathrm{x}}^{\mathrm{rec}}/\mathrm{P}_{\mathrm{z}}^{\mathrm{rec}}$	0
$\mathrm{y}^{\mathrm{rec}}, \mathrm{y}^{\Upsilon}$	$-\ \mathrm{P}_{\mathrm{y}}^{\mathrm{rec}}/\mathrm{P}_{\mathrm{z}}^{\mathrm{rec}}$	0
$\mathrm{x}^{\mathrm{opp}}, \mathrm{x}^{\Upsilon}$	0	$-\ \mathrm{P}_{\mathrm{x}}^{\mathrm{opp}}/\mathrm{P}_{\mathrm{z}}^{\mathrm{opp}}$
$\mathrm{y}^{\mathrm{opp}}, \mathrm{y}^{\Upsilon}$	0	$-\ \mathrm{P}_{\mathrm{y}}^{\mathrm{opp}}/\mathrm{P}_{\mathrm{z}}^{\mathrm{opp}}$
$\mathrm{z}^{\mathrm{opp}}, \mathrm{z}^{\mathrm{rec}}$	1	-1

Table 8: Derivatives of the combined fit constraints with respect to the lifetimes unknowns $\mathrm{L}_{\mathrm{z}}^{\mathrm{rec}}$ and $\mathrm{L}_{\mathrm{z}}^{\mathrm{opp}}$.

Constraint	$\frac{\partial F}{\partial \mathrm{x}^{\mathrm{rec}}}$	$\frac{\partial F}{\partial \mathrm{y}^{\mathrm{rec}}}$	$\frac{\partial F}{\partial \mathrm{z}^{\mathrm{rec}}}$	$\frac{\partial F}{\partial \mathrm{x}^{\Upsilon}}$	$\frac{\partial F}{\partial \mathrm{y}^{\Upsilon}}$	$\frac{\partial F}{\partial \mathrm{x}^{\mathrm{opp}}}$	$\frac{\partial F}{\partial \mathrm{y}^{\mathrm{opp}}}$	$\frac{\partial F}{\partial \mathrm{z}^{\mathrm{opp}}}$
$\mathrm{x}^{\mathrm{rec}}, \mathrm{x}^{\Upsilon}$	1	0	0	-1	0	0	0	0
$\mathrm{y}^{\mathrm{rec}}, \mathrm{y}^{\Upsilon}$	0	1	0	0	-1	0	0	0
$\mathrm{x}^{\mathrm{opp}}, \mathrm{x}^{\Upsilon}$	0	0	0	-1	0	1	0	0
$\mathrm{y}^{\mathrm{opp}}, \mathrm{y}^{\Upsilon}$	0	0	0	0	-1	0	1	0
$\mathrm{z}^{\mathrm{opp}}, \mathrm{z}^{\mathrm{rec}}$	0	0	-1	0	0	0	0	1

Table 9: Derivatives of the combined fit constraints with respect to vertex and beam spot parameters.

It it interesting to remark that this fit can applied in channels of interest for CP violation. In such channels ($\pi^+\pi^-$, $\rho\pi$, ψK^0, etc...) a $\mathrm{B}^0/\overline{\mathrm{B}^0}$ candidate has been reconstructed and a combined fit can be performed. A cut on the probability of this fit could remove a significant amount of background.

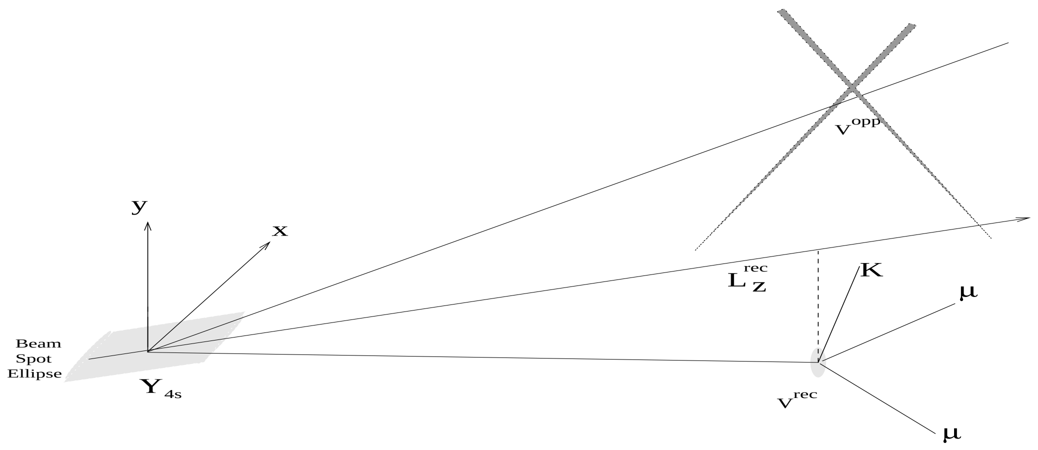

Figure 10: Same as Fig.1, when the opposite vertex V^{opp} is replaced by one or more opposite tracks. The fit intersects the line of flight of the opposite B with these tracks. The first line of flight passes through the fitted position of the vertex V^{rec} of the reconstructed B. The fit constraints also the Υ_{4S} point, origin of the lines of flight to belong the beam spot ellipse. The directions of these lines are known from kinematics. The shaded area around V^{opp} and the trajectories represents the errors made on them, and the shaded area around Υ_{4S} the beam spot ribbon.

.3.1 Variante with reconstructed vertex and a single opposite track

In this variante we replace the *opposite* vertex whose position has been calculated by the preliminary geometrical fit. One can connect directly tracks belonging to it to the beam spot and to the vertex on the *reconstructed* side. The position of V^{opp} can be parametrized as a function of the two unknowns decay paths $\mathrm{L_z^{rec}}$ and $\mathrm{L_z^{opp}}$:

$$\mathrm{x^{opp}} = \mathrm{x}^{\Upsilon} + \frac{\mathrm{P_x^{opp}}}{\mathrm{P_z^{opp}}}\mathrm{L_z^{opp}}$$

$$\mathrm{y^{opp}} = \mathrm{y}^{\Upsilon} + \frac{\mathrm{P_y^{opp}}}{\mathrm{P_z^{opp}}}\mathrm{L_z^{opp}}$$

$$\mathrm{z^{opp}} = \mathrm{z^{rec}} - \mathrm{L_z^{rec}} + \mathrm{L_z^{opp}}$$

Each of the *opposite* trajectory i is forced to pass by this point:

$$\mathrm{y}^{\Upsilon}\cos\varphi_{\mathrm{i}} - \mathrm{x}^{\Upsilon}\sin\varphi_{\mathrm{i}} + \left(\frac{\mathrm{P_y^{opp}}}{\mathrm{P_z^{opp}}}\cos\varphi_{\mathrm{i}} - \frac{\mathrm{P_x^{opp}}}{\mathrm{P_z^{opp}}}\sin\varphi_{\mathrm{i}}\right)\mathrm{L_z^{opp}} + \mathrm{d_i^0} = 0 \tag{21}$$

$$\mathrm{z^{rec}} - \mathrm{L_z^{rec}} + \mathrm{L_z^{opp}} - \mathrm{Z_i^0} - \mathrm{tg}\theta_{\mathrm{i}}(\mathrm{x}^{\Upsilon}\cos\varphi_{\mathrm{i}} + \mathrm{y}^{\Upsilon}\sin\varphi_{\mathrm{i}}) - \mathrm{tg}\theta_{\mathrm{i}}\left(\frac{\mathrm{P_x^{opp}}}{\mathrm{P_z^{opp}}}\cos\varphi_{\mathrm{i}} + \frac{\mathrm{P_y^{opp}}}{\mathrm{P_z^{opp}}}\sin\varphi_{\mathrm{i}}\right) = 0 \tag{22}$$

In addition to these 2 contraints per *connected* track, one has on the *reconstructed* side:

$$\mathrm{x^{rec}} - \mathrm{x}^{\Upsilon} - \frac{\mathrm{P_x^{rec}}}{\mathrm{P_z^{rec}}}\mathrm{L_z^{rec}} = 0 \tag{23}$$

$$\mathrm{y^{rec}} - \mathrm{y^{\Upsilon}} - \frac{\mathrm{P_y^{rec}}}{\mathrm{P_z^{rec}}}\mathrm{L_z^{rec}} = 0 \tag{24}$$

Only one track is necessary to obtain the *opposite* decay point. In that case the fit is only 1-C. In the lifetime analysis, it has been used to remove *secondary* charm tracks or K_s^0 decay products, when the geometrical vertexing of the *opposite* B has failed. But ultimately, it can used by including all opposite tracks. In this case one fits directly an opposite vertex compatible with the lines of flight, bypassing the intemediate step of an independant vertexing. This has not been explored at this stage.

.4 Other applications

Other applications have been recently developped. γs and π^0s have been introduced in kinematical fits. This allows to perform D^0, $D^{\pm}$ vertexing with the D mass constraint with and without π^0s. With the purpose of using in the future for the lifetimes decay channels $B \to D^{*0}+X$, $B \to D^{*\pm}+X$, which are much more frequent than the $B \to \psi+X$ channels, a geometric and kinematical fit of a B vertex involving D^* has been implemented. These extensions are not described here

.5 Adaptation to C^{++}

A preliminary adaptation of the FORTRAN code in C++ has been made. It is foreseen to further adapt this code, in such a way that it can be used as a BABAR fitting tool. At the time beeing, it a set of classes called *GminSqFit*, intended to become a package. The mnemonic *GminSq* stands for *generalizedleastsquare*, since the fits are least square minimisations of parameters, with unknowns and constraints.

.5.1 Class *GminSqFit*: Fit definition

This class provides the interface allowing the user to define the type of fit to be performed. The fit is an object, made of groups of parameters, unknowns and constraints.
The setting up of a fit can be viewed like the assembling of building blocks. It is first required to set the different groups of parameters, and the initial values of the unknowns. Once parameters and unknowns are introduced, it is necessary to define the constraints. For the time being 5 types of constraints has been considered: geometric trajectory constraints(method *addGeometric*) ; Mass constraints (method *addKinematic*); Beam energy constraint(method *addEnergyBeam*); Beam spot constraints of Eq.(16-17) (method *addBeamSpot*); Combined fit constraints of Eq.(16-19) (method *addVxBack*). Each method computes the array of initial constraint values $F(\hat{q},\hat{\eta})_r$ and the matrices of derivatives of constraints r with respect to parameters q and unknowns η.

At this stage, the fit is ready to be executed. A method, called *MakeFit* set links with the class *GminSqGenFit* which actually performs the fit. After the execution, a method (called *GetFit*) return an object (*GminSqGenFit*) giving acces to the results.

.5.2 Class *GminSqGenFit*: Fit calculation

This class performs the fit itself. Three different constructors have been made. The first and second ones do not compute the error matrix on the fitted parameters which is not always used but long to calculate. The third constructor provides this error matrix.

.5.3 Class $GminSqFitParam$: Creation of groups of parameters

In general, parameters are not correlated from group to group. So error matrices are block diagonal if we put parameters in a correct order. For example, such structures of groups of parameters appears naturally when we have different tracks. The class $GminSqFitParam$ defines objects which contain a group of parameters and its error matrix. Such objects can be created by giving directly the parameters (like beam spot data or vertex coordinates) or standard values of track parameters naturally associated to a *BtaCandidate.* Actually this version used only charged tracks. In the future, it will also include neutrals π^0s, γs, K_s^0s .

.5.4 Class *GminSqPtools*: Fit Tools for constraints

This class contains tools to calculate various derivatives of the quadrimomentum components with respect to the tracks parameters (for kinematical contraints). It is also used to store the particle energy and momentum in the class $GminSqFitParam$.

.5.5 Class $BlockDiagMatrix$: Acceleration of matrices manipulations

Most of the matrices calculated during the fit are block diagonal. In order to accelerate calculus, a class of such objects has been build. It contains algebraic tools optimized for the multiplication and inversion of such matrices, and methods to assure compatibility with standard matrices classes.